Journal of Visualized Experiments
Use of 3D Robotic Ultrasound for in vivo Analysis of Mouse Kidneys
--Manuscript Draft--

Article Type:	Invited Methods Collection - JoVE Produced Video
Manuscript Number:	JoVE62682R2
Full Title:	Use of 3D Robotic Ultrasound for in vivo Analysis of Mouse Kidneys
Corresponding Author:	Michael F. Romero Mayo Clinic College of Medicine and Science Rochester, Minnesota UNITED STATES
Corresponding Author's Institution:	Mayo Clinic College of Medicine and Science
Corresponding Author E-Mail:	Romero.Michael@mayo.edu
Order of Authors:	Michael F. Romero
	Heather L. Holmes
	Alison A. Stiller
	Adriana V. Gregory
	Carolyn M. Roos
	Jordan D. Miller
	Christopher J. Moore
	Ryan C. Gesser
	Tomasz J. Czernuszewicz
	Timothy L. Kline
Additional Information:	
Question	Response
Please specify the section of the submitted manuscript.	Medicine
Please indicate whether this article will be Standard Access or Open Access.	Standard Access ($1400)
Please indicate the **city, state/province, and country** where this article will be **filmed**. Please do not use abbreviations.	Rochester, Minnesota, United States
Please confirm that you have read and agree to the terms and conditions of the author license agreement that applies below:	I agree to the Author License Agreement
Please provide any comments to the journal here.	
Please confirm that you have read and agree to the terms and conditions of the video release that applies below:	I agree to the Video Release

1 **TITLE:**
2 Use of 3D Robotic Ultrasound for *In Vivo* Analysis of Mouse Kidneys
3
4 **AUTHORS AND AFFILIATIONS:**
5 Heather L. Holmes[1*], Alison A. Stiller[1*], Christopher J. Moore[4], Adriana V. Gregory[2], Carolyn M.
6 Roos[3], Jordan D. Miller[1,3], Ryan C. Gessner[4], Tomasz J. Czernuszewicz[4], Timothy L. Kline[2], Michael
7 F. Romero[1,5]
8
9 [1]Physiology & Biomedical Engineering, [2]Radiology, [3]Surgery, [5]Nephrology & Hypertension, Mayo
10 Clinic, Rochester, MN, USA
11 [4]SonoVol, Inc., Durham, NC, USA
12
13 *These authors have contributed equally.
14
15 Email addresses of co-authors:
16 Heather L. Holmes   (holmes.heather2@mayo.edu)
17 Alison A. Stiller   (stiller.alison@mayo.edu)
18 Christopher J. Moore   (chris.moore@sonovol.com)
19 Adriana V. Gregory   (gregory.adriana@mayo.edu)
20 Carolyn M. Roos   (roos.carolyn@mayo.edu)
21 Jordan D. Miller   (miller.jordan@mayo.edu)
22 Ryan C. Gessner   (ryan.gessner@sonovol.com)
23 Tomasz J. Czernuszewicz   (tomekc@sonovol.com)
24 Timothy L. Kline   (kline.timothy@mayo.edu)
25 Michael F. Romero   (romero.michael@mayo.edu)
26
27 **Corresponding author:**
28 Michael F. Romero   (romero.michael@mayo.edu)
29

30 **SUMMARY:**
31 This protocol demonstrates robotic ultrasound (US) as a practical, cost-effective, and quick
32 alternative to traditional non-invasive image modalities.
33
34 **ABSTRACT:**
35 Common modalities for *in vivo* imaging of rodents include positron emission tomography (PET),
36 computed tomography (CT), magnetic resonance imaging (MRI), and ultrasound (US). Each
37 method has limitations and advantages, including availability, ease of use, cost, size, and the use
38 of ionizing radiation or magnetic fields. This protocol describes the use of 3D robotic US for *in*
39 *vivo* imaging of rodent kidneys and heart, subsequent data analysis, and possible research
40 applications. Practical applications of robotic US are the quantification of total kidney volume
41 (TKV), as well as the measurement of cysts, tumors, and vasculature. Although the resolution is
42 not as high as other modalities, robotic US allows for more practical high throughput data
43 collection. Furthermore, using US M-mode imaging, cardiac function may be quantified. Since
44 the kidneys receive 20%–25% of the cardiac output, assessing cardiac function is critical to the

45 understanding of kidney physiology and pathophysiology.
46
47 **INTRODUCTION:**
48 The most common modalities for *in vivo* rodent imaging include positron emission tomography
49 (PET), optical imaging (OI), computed tomography (CT), magnetic resonance imaging (MRI), and
50 ultrasound (US). These techniques provide high-resolution *in vivo* images, allowing investigators
51 to quantitatively assess and longitudinally follow disease models non-invasively[1]. While each
52 imaging modality has limitations, they also provide invaluable tools for preclinical research.
53
54 Here, the study details a US system and presents the protocol for robotic and 3D rodent imaging.
55 US waves are produced by a probe called a transducer, which is typically hand-held. Sound waves
56 are reflected back as they interact with tissues, and the echoes are reconstructed into images[2].
57 The protocol described here will focus on kidney and cardiac imaging using a robotically
58 controlled transducer and using software that allows rapid 3D reconstruction for quantitative
59 assessment.
60
61 Robotic US is a fast, reliable, and non-invasive imaging modality that allows investigators to
62 conduct high-throughput and longitudinal studies. Compared to hand-held US methods, the
63 robotic US method is time-efficient, as up to three animals can be scanned in a matter of minutes.
64 High throughput for kidney measurements suggests that up to 20 mice per hour may be imaged.
65 The robotic transducers are located underneath the acoustic membranes and move
66 independently of the animal with two degrees of freedom (**Figure 1A**). This allows novice users
67 to obtain high-quality images, whereas hand-held US methods are more susceptible to user error.
68 The coupled software allows efficient, real-time 3D kidney reconstruction. Previously, magnetic
69 resonance imaging (MRI) has been a prevalent method for non-invasive imaging due to the
70 excellent soft-tissue contrast, lack of radioactivity, and penetration depth. However, MRI often
71 requires long acquisition times and is costly to perform. US has been evaluated as a reliable and
72 more rapid alternative to MRI in assessing total kidney volume (TKV)[3].
73
74 **PROTOCOL:**
75
76 All the steps in this protocol comply with the Mayo Clinic (Rochester, MN) animal use guidelines.
77
78 **1. Animal model**
79
80 1.1. Obtain mice from commercial sources.
81
82 NOTE: C57BK6j (age = 18 months; n = 22 (7 males, 15 females)) (**Table of Materials**) and
83 Pkd1$^{(RC/RC)}$ (age = 18 months; n = 9 (3 males, 6 females))[4] were used for the study.
84
85 **2. Hair removal**
86
87 2.1. Anesthetize the animal using vaporized isoflurane (2%–3%) in an anesthesia chamber.
88 Ensure that the animal is sufficiently anesthetized by performing a toe pinch. Ensure that the

89 mouse is breathing at a rate of approximately 60–90 breaths/min without obvious air gulping.
90
91 NOTE: Vaporized isoflurane was chosen due to the ability to control and fine-tune the animal's
92 level of anesthesia.
93
94 2.2.   Use an electric razor to shave the desired skin area for US measurements.
95
96 NOTE: In this study, the focus is on kidney and cardiac measurements, so the animal's chest and
97 back were shaved.
98
99 2.3.   Apply the depilatory cream to the animal's shaved skin with a cotton-tipped applicator.
100 Wipe the cream off after 30–60 s using a dry paper towel. Then, continue to wipe away depilatory
101 cream residue using wet gauze pads. Ensure the hair removal is complete prior to beginning
102 scans.
103
104 NOTE: The remaining hair will interfere with the image quality; complete hair removal is crucial.
105 However, it is necessary to wipe the depilatory cream off within a minute to prevent injuring the
106 animal's skin. Leftover depilatory cream on the animal can stain the imaging membrane of the
107 US machine. Ensure proper cleaning of the animal using wet gauze pads.
108
109 **3.   Animal positioning**
110
111 3.1.   Turn on the US machine and the heat lamp above the US platform. Turn on the
112 appropriate anesthesia valves for the corresponding US bays.
113
114 NOTE: The US machine must be turned on prior to starting the imaging US software.
115
116 3.2.   Fill the bays with enough water to cover the membrane. Place the anesthetized animal in
117 the nose cone.
118
119 3.2.1. For cardiac measurements, place the animal in a prone position and angle it
120 approximately 30° to the right.
121
122 3.2.2. For kidney measurements, place the animal in a straight and supine position. Gently
123 flatten the animal's body to minimize the air pockets between the animal and the membrane
124 (**Figure 1B**).
125
126 NOTE: Running a finger alongside the animal's body can remove any air bubbles adhering to the
127 skin, which will interfere with imaging. Use water or US saline gel as US medium; but water
128 facilitates the rapid imaging discussed here.
129
130 **4.   Ultrasound measurements**
131
132 4.1.   In the imaging US software, select **US Acquisition** and allow the instrument to initialize.

133
134 4.2. Kidney Imaging using B-mode.
135
136 4.2.1. Enter a name for the study in the appropriate dialog box.
137
138 4.2.2. Enter the animal ID in the appropriate dialog box.
139
140 NOTE: Up to three animals can be imaged sequentially.
141
142 4.2.3. Click on the tab labeled **3D** to initialize 3D scanning.
143
144 4.2.4. Using the live camera feed, move the region of interest (ROI) box to contain the kidneys.
145
146 NOTE: The size of the ROI may be adjusted depending on the size of the image target. Increasing
147 the size of the ROI will slightly increase the scan time (**Figure 1C**). Depending on ROI size, the
148 scanner will automatically adjust the number of passes required for the transducer to scan the
149 entire ROI.
150
151 4.2.5. Depending on the type of image desired, select **Linear Array** or **Wobbler**, to choose the
152 transducer. Select from **Fast Scan** or **Optimized** for either transducer.
153
154 NOTE: Linear array is faster and usually provides adequate imaging. The wobbler transducer can
155 be utilized if unable to acquire the desired image quality with the linear array. The wobbler
156 transducer utilizes a higher frequency wavelength and therefore provides more definition in
157 images. The Fast Scan option acquires medium quality images with no breathing correction at a
158 higher speed. While the Optimized option requires slightly more time, it provides better image
159 quality and allows for breathing correction. This manuscript will focus on using the Optimized
160 linear array preset.
161
162 4.2.6. Click on the **Live View** to see a live image of the desired viewing area.
163
164 4.2.7. To move the transducer, click on the circular **Go To** button, and then click on the area of
165 the mouse to be imaged. Use the directional arrows with predetermined step sizes to finely
166 adjust the transducer position.
167
168 4.2.8. Click on the arrow at the side of the **Control Panel** window to open the **Settings Tray**.
169 Click on **Scan Protocol** to open scanning settings.
170
171 4.2.9. Determine the ideal focal depth and adjust the sliders for the TGC (time gain
172 compensation) to change the image contrast to best view the kidneys. After achieving the desired
173 settings, click on the arrow again to close the **Settings Tray**.
174
175 4.2.10. Press the **Acquire Static** button to commence 3D scanning.
176

177   NOTE: Progress of the scan is indicated via a progress bar in the bottom left of the software.
178
179   4.2.11. Once the scanning is complete, check the image quality by clicking on the blue download
180   arrow to open the scan in **Preview Mode**. Move through the 3D frames of the scan by dragging
181   the red arrow at the top of the window. To zoom in or out, hold the **Ctrl** key and use the scroll
182   button on the mouse.
183
184   4.2.12. To scan additional animals, refresh the animal ID dialog boxes, input the new IDs, and
185   then repeat the above steps.
186
187   4.3.   Cardiac imaging using M mode.
188
189   NOTE: M-mode is the display of an ultrasound wave along a specific, chosen ultrasound line.
190
191   4.3.1.   Click on the **M Mode** tab to activate cardiac imaging.
192
193   NOTE: Only one animal can be imaged at a time.
194
195   4.3.2.   Ensure that the animal is in the appropriate position for cardiac scans (step 2.2). Move
196   the ROI to the approximate location of the heart.
197
198   4.3.3.   Push the **Heart Finder** button to locate the heart. Use the heat map to optimize the
199   location of the transducer. Use the circular **Go To** button to move the transducer to the left
200   ventricle (**Figure 2A**).
201
202   4.3.4.   Go to the **Live View** and use the arrow buttons to place the transducer between the
203   papillary muscles (**Figure 2B**). To verify the proper placement of the transducer, view the live M
204   Mode trace (**Figure 2D**).
205
206   4.3.5.   Once the transducer is in the appropriate position, click on **Acquire Sequence**. Click on
207   the blue download arrow to view the completed scan.
208
209   **5.   Kidney analysis (mechanics of analysis)**
210
211   5.1.   Open the **Image Analysis** tab and select the **Load Volume(s)** button to input the image
212   files/folders.
213
214   5.1.1.   Segmentation
215
216   5.1.1.1.   Move the colored lines representing various planes to find the kidney in all the
217   planes.
218
219   5.1.1.2.   Click on **Add** to add a new segmentation. Provide a markup name for the file.
220

221 <mark>5.1.1.3.   Use the **Surface Cut** button to add points around the outer edge of the kidney in</mark>
222 <mark>multiple planes. Click on **Apply** to generate segmentation through the entire kidney (**Figure 3A**).</mark>
223
224 <mark>5.1.1.4.   Scroll through the different frames in each plane and edit any inaccurate regions</mark>
225 <mark>by clicking on **Edit** and dragging the points to the correct location.</mark>
226
227 5.1.1.5.   Alternatively, if the kidney is irregular in shape, use the **Draw** function to create
228 an irregularly shaped trace around the kidney. Either click points around the edge or hold the left
229 click to draw the trace freehand.
230
231 5.1.1.6.   To complete the trace with the **Draw** button, right-click with the mouse. Scroll
232 ahead multiple frames and repeat the tracing process.
233
234 5.1.1.7.   Repeat until the frames are traced throughout the entire region of interest.
235
236 5.1.1.8.   If the **Draw** function is used, select **Fill Between Slices** to check and adjust the
237 trace. Click on **Initialize** to see a preview. If the preview is acceptable, click on **Apply**. If not, click
238 on **Cancel** and modify the tracings.
239
240 NOTE: The **Erase** button will allow deletion of a region within a trace. The **Smooth** button
241 smooths the jagged edges of a trace.
242
243 5.1.1.9.   When image analysis is satisfactory, select **Save** to save the analysis to the original
244 image file.
245
246 5.1.2. Measurement
247
248 5.1.2.1.   Use the **Calipers** function to measure features within the image. Click on the
249 **Calipers** button and left click the two points of the distance to be measured (**Figure 3B**).
250
251 5.1.2.2.   Save the measurement by clicking the disk button at the top of the screen.
252
253 <mark>6.   **Cardiac analysis**</mark>
254
255 6.1.   Select **Load Volumes** to input the file(s) to analyze.
256
257 6.2.   Select the **Add** option.
258
259 <mark>6.3.   Use the **Point Placement** tool to trace the systole and diastole for each layer of heart</mark>
260 <mark>tissue. Continue with the other layers of heart tissue. Use the **Edit** function to modify the traces</mark>
261 <mark>(**Figure 2C,D**).</mark>
262
263 NOTE: If the M-mode trace is very clear, use the **Add (auto)** button to automatically generate
264 tracings of each layer.

265

266 6.4.   Select **Apply** to calculate the cardiac parameters. View the **Quantify** tab and select **Export**
267 **Statistics** to export all data as a *.csv file (**Figure 2E**).

268

269 **REPRESENTATIVE RESULTS:**
270 **Results of kidney analysis**
271 Surface area and volume data are acquired from the segmentation of the kidneys. This
272 information can be used to compare experimental and control models or track changes over
273 time. The calipers tool is useful for quickly measuring abnormalities (i.e., cysts, tumors) and how
274 they change in length over time. **Figure 3** suggests that both the segmentation and caliper
275 methods can be used to measure cyst volumes accurately. **Figure 4** demonstrates a clear
276 difference in total kidney volume (TKV) between age-matched control and experimental
277 (*Pkd1$^{RC/RC}$*) mice. 3D visualization of these volume renderings may be performed within the
278 system, including rotations within 3D space (
279 **Figure 5**). These 3D-reconstructions are then used to calculate TKV (mm^3; **Figure 4**) as well as
280 individual large cyst volume.

281

282 **Results of cardiac analysis**
283 Many useful parameters are acquired from the analysis of M Mode images. These data provide
284 a good snapshot of the left ventricular (LV) cardiac function at that point in time. The data output
285 includes LV internal diameter, LV posterior wall, LV anterior wall diameter, ejection fraction,
286 fractional shortening, stroke volume, heart rate, cardiac output, LV volume, and LV mass. The
287 success of cardiac analysis is dependent on accurate segmentation of the layers on the M Mode
288 image. Most cardiovascular results are calculated by the peak systolic and diastolic phases of the
289 posterior and anterior endocardial layers. The posterior epicardial layer appears bright white and
290 follows a similar pattern to the posterior endocardial layer. The tracing for the posterior
291 endocardial layer should be placed on the lowest contour. The anterior endocardial layer should
292 be traced along the highest contour of that layer. The anterior epicardial layer appears linear at
293 the bottom of the image due to the prone positioning of the animal (**Figure 2D**). **Figure 4** shows
294 an example of one study with no significant difference in cardiac output between experimental
295 and control mice. As with renal imaging, 3D cardiac visualization is possible. Nevertheless, a 4D
296 visualization of the cardiac cycle (**Supplemental Figure 1**) allows the investigator to visualize and
297 pinpoint both morphologic and cycle-dynamic abnormalities in the assessed animal.

298

299 **Morphology assessment**
300 For quick and inexpensive assessment, ultrasound can effectively monitor physiological
301 parameters longitudinally. However, many studies wish to additionally determine finer
302 morphologic characteristics, e.g., number and sizes of cysts, calcifications (kidney stones),
303 vascularization, or degree of fibrosis. **Figure 5** compares a normal mouse kidney to a cystic mouse
304 kidney to a moderately calcified mouse kidney. By increasing the ultrasound center frequency
305 (10 MHz with the linear array) to 35 MHz (wobbler amplifier), pictures of increasing detail may
306 be obtained.

307

308 **FIGURE AND TABLE LEGENDS:**

Figure 1: Ultrasound system and mouse placement. (**A**) Diagram of ultrasound system and location of transducers. (**B**) View of mice in supine position on ultrasound platform with heat lamp. (**C**) Example of region of interest (ROI)s in place for area of interest (kidneys) with animal IDs.

Figure 2: Cardiac ultrasound imaging to obtain physiological parameters. (**A**) Use of the **Heart Finder** heatmap image to position the transducer in the left ventricle for M-Mode imaging. The heart is indicated by the large green dot. (**B**) View of the transducer when placed correctly over papillary muscles (dotted box). (**C**) Example view of layers needed to measure cardiac parameters. (**D**) View of live M-Mode image with layers designated as in panel C. (Layers from top to bottom: posterior epicardial, posterior endocardial, anterior endocardial, and anterior epicardial.) (**E**) Example output of statistics generated from cardiac measurements.

Figure 3: Using segmentation and calipers tools to measure kidneys and cyst. (**A**) Example segmentations of both kidneys (blue and orange shading) and a large cyst (yellow) with volumes listed below. Non-segmented views are shown underneath so that the unobscured US may be viewed. (**B**) Example use of calipers to measure the same cyst from **Figure 3A** with measurements below. The volume was calculated using the formula for an ellipse (volume = $(4/3)\pi$ x a x b x c, where a, b, c are relative x, y, z, respectively).

Figure 4: TKV distributions of WT and cystic mouse kidneys. Representation of TKVs for WT and diseased (Pkd1$^{RC/RC}$) mice. n = 22 (WT) n = 9 (PKD1$^{RC/RC}$); Results of two-tailed *t*-test: p < 0.0001. Box shows 25–75th percentile values.

Figure 5: Animated 3D reconstruction of segmented kidneys and cyst. Using the software, the 3D projections of the kidneys and cyst may be rotated or rocked in the 3D space (blue = left kidney; yellow = large cyst; orange = right kidney).

Figure 4: Cardiac physiological parameters from US measurements. Representation of cardiac output (mL/min) for WT and diseased (Pkd1$^{RC/RC}$) mice. n = 22 (WT) n = 9 (Pkd1$^{RC/RC}$). The lower tabulated data show that there is no significant difference for these two groups in ejection fraction, stroke volume, heart rate (HR), or cardiac output (CO). Results of two-tailed *t*-test: p > 0.05. Box shows 25–75th percentile values.

Figure 5: Comparison of US Sagittal sections of normal and two pathologies. (**A**) Wild-type (C57BK6j strain) kidney (TKV = 143.202 mm^3). (**B**) Cystic kidney with increased TKV (Pkd1$^{RC/RC}$ mouse) (TKV = 333.158 mm^3). Cysts are indicated by yellow arrows. (**C**) Kidney with vascular calcifications (Model = Low-Density Lipoprotein Receptor Deficient, Apolipoprotein B100-only mouse fed a Western diet for 12 months[5]) (TKV = 127.376 mm^3). Renal stones are indicated by green arrows.

Supplemental Figure 1: 4D cardiac cycle movie from US measurements. Using the software, a representation of the beating heart is captured in 3D US and projected through the cardiac cycle. The green arrow indicates the aortic valve. (Model = Low-Density Lipoprotein Receptor Deficient,

353 Apolipoprotein B100-only mouse, fed a Western diet for 12 months[5]). This model generates
354 vascular calcifications enabling easier visualization of the heart and valves due to the greater
355 acoustic reflectivity of the calcifications in US. Similar 4D reconstructions are possible with WT
356 mice; however, the captured acoustic contrast will not be as high.
357
358 **DISCUSSION:**
359 Ultrasound utilizes sound waves, and any barriers to sound wave propagation will interfere with
360 image quality. Thus, complete hair removal of the area to be imaged is critical. It is also important
361 to ensure complete removal of depilatory cream as it can cause burns/irritation of the animal's
362 skin and discolor the transparent membrane of the scanner. Adequate water levels in the bays
363 are necessary for optimal sound wave propagation, thus required for obtaining the highest image
364 resolution. However, when the animal is in a prone position, ensure the animal's snout is above
365 the water level or the animal is at risk of water inhalation. Optimization of imaging parameters,
366 especially focal depth, is critical for obtaining high-quality images. Modifications to parameters
367 may be necessary for individual animals.
368
369 Robotic US provides many advantages over traditional hand-held US modalities. First, the system
370 uses a simple point-and-click camera-based interface. This feature addresses the complexity of
371 conventional US and produces consistent data even when operated by a novice user[6]. Second,
372 the system allows the use of water rather than traditional US gel as an acoustic medium.
373 Previously, the use of US gel allowed the formation of bubbles that interfered with quality image
374 acquisition. Also, the US gel is messy and provides challenges for clean-up. Further, the water is
375 warmed by the heat lamp and helps maintain the animal's body temperature. Third, the robotic
376 US is faster, so artifacts from respiratory motion are not problematic. The increased imaging
377 speed allows for the practical completion of high throughput data collection. Fourth, the robotic
378 US obtains 3D images, and therefore makes 3D reconstruction of objects simple (
379 **Figure**). MRI and other modalities are expensive, time-consuming, and not always available.
380 Importantly, the robotic US system fits on a table or bench and is more cost-efficient. Finally,
381 prior work demonstrated that robotic US could provide comparable measurement data to more
382 expensive modalities, such as MRI[3].
383
384 While the image quality and resolution of the robotic US system described in this work were
385 adequate for the proposed application (**Figure 5**), there are several ways that image quality can
386 be improved in the future. For instance, utilizing higher frequency transducers (e.g., 50–70 MHz)
387 would result in higher resolution images with better feature definition. While utilizing higher
388 frequencies would result in a poorer depth of penetration, the images should be sufficient for *in*
389 *vivo* imaging of superficial organs, such as the mouse kidney. As with other imaging modalities,
390 contrast agents may be used to enhance specific features. For US, this typically means using
391 something highly reflective of sound waves. Intravascular microbubbles in which lipids surround
392 very small gas bubbles are one such agent. The micron-sized gas bubbles are highly reflective and
393 thus provide a second distinct signal that translates into a high-resolution of vasculature[7]. While
394 this acoustic contrast technique may be quite useful, it can have several downsides. First, the
395 microbubbles must be made fresh and only persist *in vivo* for 5–10 min. Second, *in vivo*
396 intravascular injection typically requires tail veil catheterization for injection, and this can be

397 technically challenging. Under certain circumstances and pulsing regimes, microbubble imaging
398 can itself lead to renal vasculature damage[8].
399
400 There are also some more general limitations of the particular US system used. First, only one
401 linear array (centered at 18 MHz) is included in the robotic chassis, so switching to higher or lower
402 frequency probes is not currently possible. This may impact the breath of models (either larger
403 or smaller) that can be evaluated with the system. Future iterations of the instrument should
404 include multiple linear arrays to cover the full range of preclinical animal models. Second, the
405 transducer angle relative to the animal subject cannot be controlled. Therefore, performing
406 angle-dependent imaging techniques, such as Doppler, or achieving alternative in-plane views of
407 certain organs (e.g., long axis view of kidney) requires repositioning of the animal and can be
408 difficult to achieve. Additional degrees-of-freedom could be added to the robotic movement to
409 ameliorate this challenge. Third, on occasion, we have observed reverberation artifacts arising
410 from the acoustic membrane that separates the animal from the transducer that can obscure
411 visualization of superficial features and boundaries. In these cases, using a gel standoff to elevate
412 the animal away from the membrane can remedy the situation. Finally, temperature control via
413 heat lamp is imprecise, and therefore close attention must be paid to the animal's core body
414 temperature while imaging. More controlled heating mechanisms, such as an integrated heating
415 pad, will likely improve homeostasis management and imaging throughput.
416
417 The use of robotic US may be applicable to various fields of research. This technology enables
418 visualization of gross tissue structures, thus may be used to track tumor progression and
419 potential therapies[6,9] as well as renal morphology as presented here. The ability to segment the
420 specific features of the images makes it an attractive tool for studying models of polycystic kidney
421 disease (PKD)[3]. M-mode images allow for simple quantification of many important cardiac
422 parameters enabling *in vivo* assessment of cardiac physiology. As the kidneys receive 20%–25%
423 of the cardiac output (Boron & Boulpaep, 2017[10]), understanding cardiac function during the
424 longitudinal assessment of renal pathology is important. Through these US protocols, we have
425 tried to illustrate that US imaging is not only practical for *in vivo* and longitudinal kidney studies
426 but also that increasingly US tools enable both morphologic as well as physiologic assessment of
427 mice in preclinical studies.
428

436 **REFERENCES:**
437 1.   Cunha, L. et al. Preclinical imaging: an essential ally in modern biosciences. *Molecular*
438 *Diagnostics & Therapy*. **18** (2), 153–173 (2014).
439 2.   NIBIB.   *Ultrasound*,   https://www.nibib.nih.gov/science-education/science-
440 topics/ultrasound#pid-936 (2016).

441 3.   Beaumont, N. J. et al. Assessing polycystic kidney disease in rodents: Comparison of
442 robotic 3d ultrasound and magnetic resonance imaging. *Kidney360*. **1** (10), 1128–1136 (2020).
443 4.   Hopp, K. et al. Functional polycystin-1 dosage governs autosomal dominant polycystic
444 kidney disease severity. *The Journal of Clinical Investigation*. **122** (11), 4257–4273 (2012).
445 5.   Weiss, R. M., Ohashi, M., Miller, J. D., Young, S. G., Heistad, D. D. Calcific aortic valve
446 stenosis in old hypercholesterolemic mice. *Circulation*. **114** (19), 2065–2069 (2006).
447 6.   Czernuszewicz, T. J. et al. A new preclinical ultrasound platform for widefield 3D imaging
448 of rodents. *Review of Scientific Instruments*. **89** (7), 075107 (2018).
449 7.   Chong, W. K., Papadopoulou, V., Dayton, P. A. Imaging with ultrasound contrast agents:
450 current status and future. *Abdominal Radiology (NY)*. **43** (4), 762–772 (2018).
451 8.   Nyankima, A. G., Kasoji, S., Cianciolo, R., Dayton, P. A., Chang, E. H. Histological and blood
452 chemistry examination of the rodent kidney after exposure to flash-replenishment ultrasound
453 contrast imaging. *Ultrasonics*. **98**, 1–6 (2019).
454 9.   Rojas, J. D. et al. Ultrasound measurement of vascular density to evaluate response to
455 anti-angiogenic therapy in renal cell carcinoma. *IEEE Transactions on Biomedical Engineering*. **66**
456 (3), 873–880 (2019).
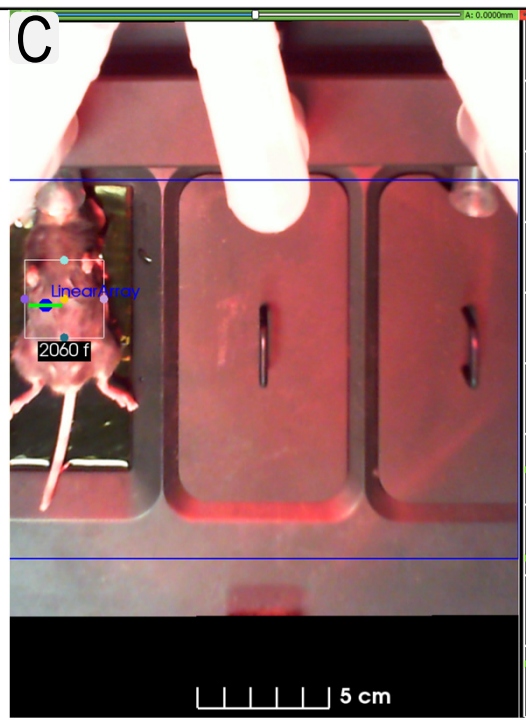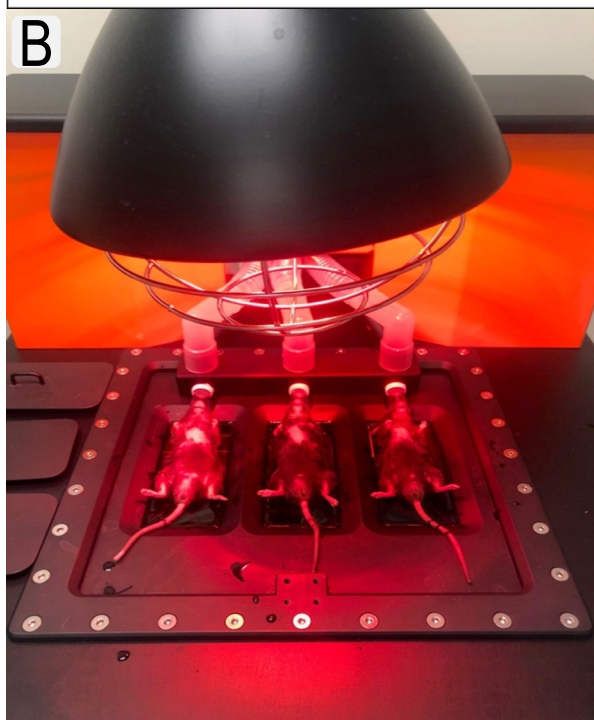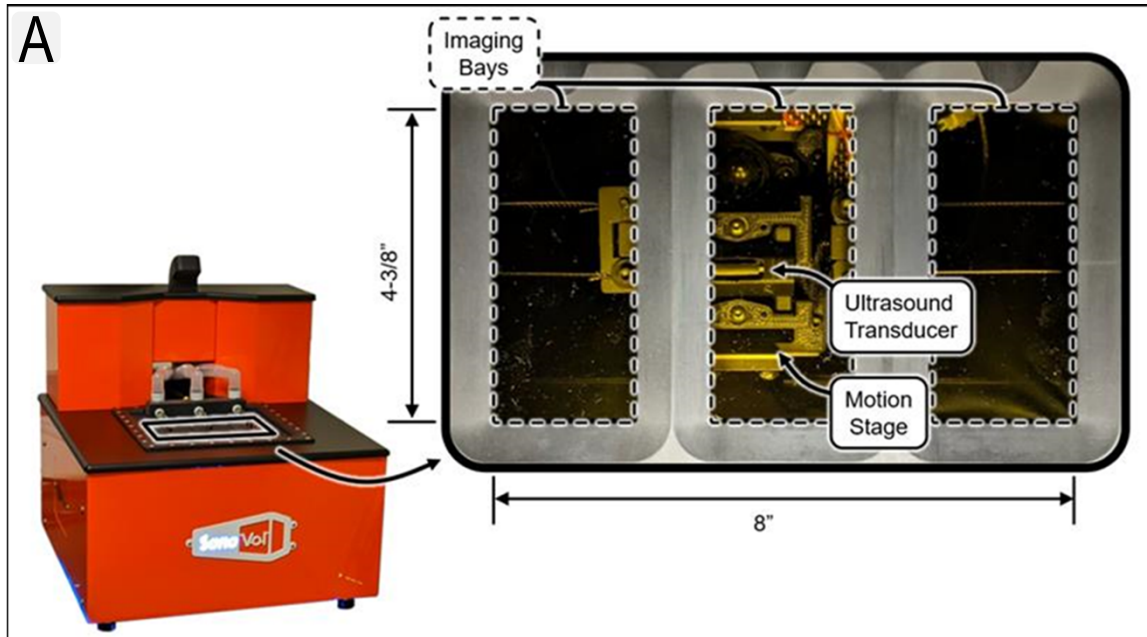457 10.   Boron, W. F., Boulpaep, E. L. *Medical Physiology*. 3rd edn, Elsevier (2017).
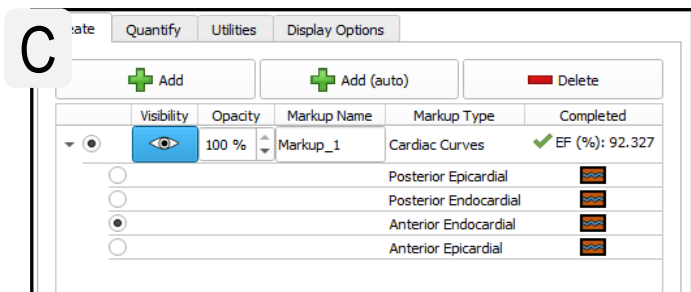458

A

Imaging Bays

4-3/8"

8"

Ultrasound Transducer

Motion Stage

SonoVol

B

C

LinearArray

2060 f

5 cm

Figure 1

Figure02

A — nearArray — 5 mm

B — S: 11.3340mm — 10 mm — 7.0 mm — Papillary muscles — 5 mm

C

	Visibility	Opacity	Markup Name	Markup Type	Completed
	👁	100 %	Markup_1	Cardiac Curves	✔ EF (%): 92.327
				Posterior Epicardial	〰
				Posterior Endocardial	〰
				Anterior Endocardial	〰
				Anterior Epicardial	〰

ate Quantify Utilities Display Options

Add   Add (auto)   Delete

D — 10 mm — 5.0 mm — 0 mm

E

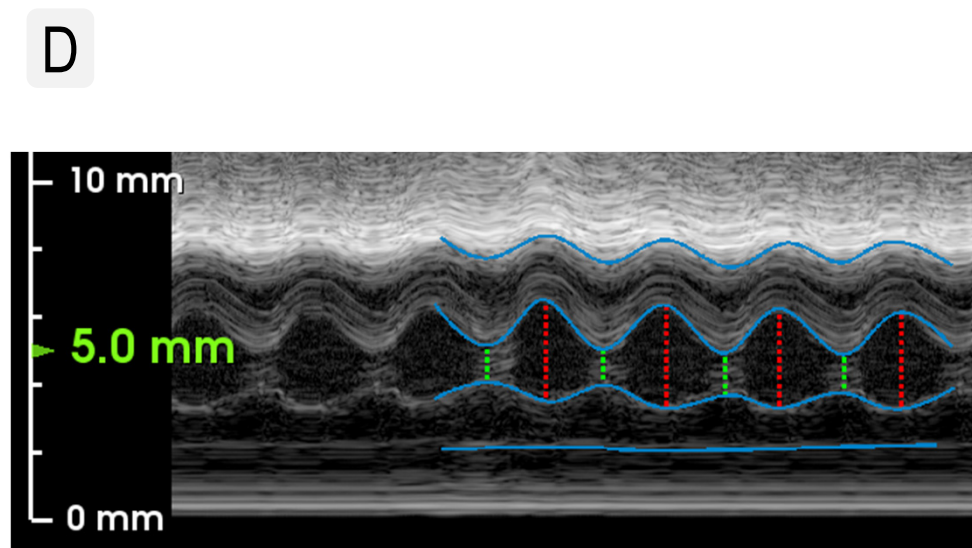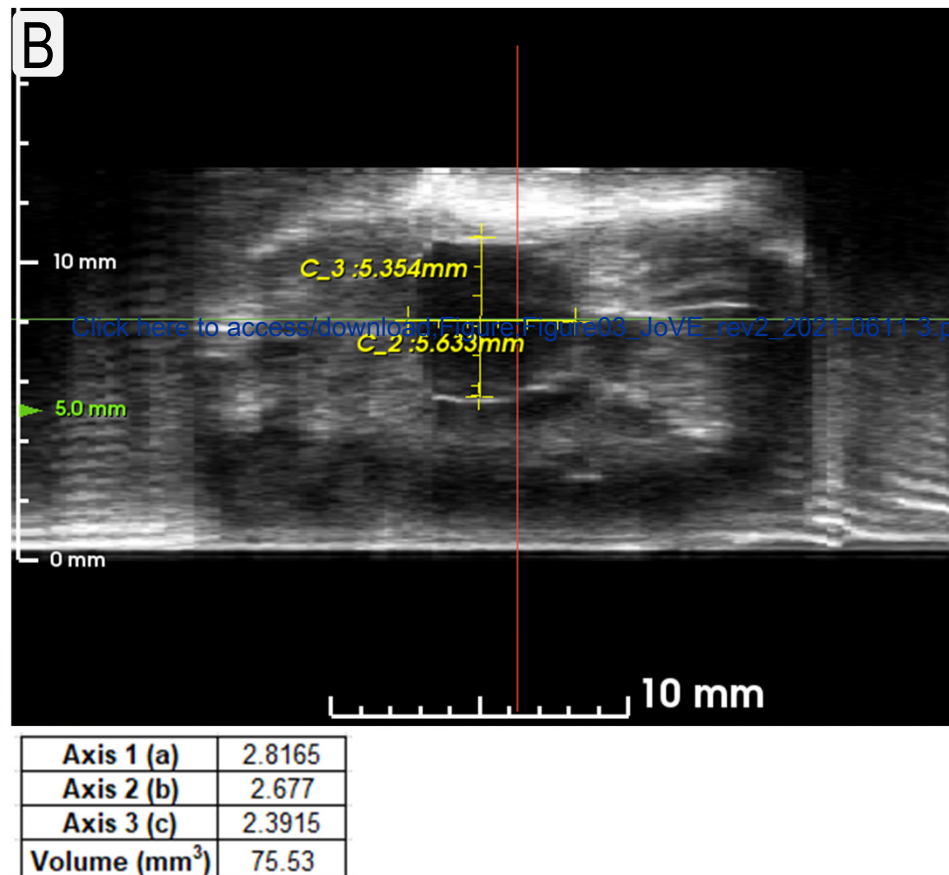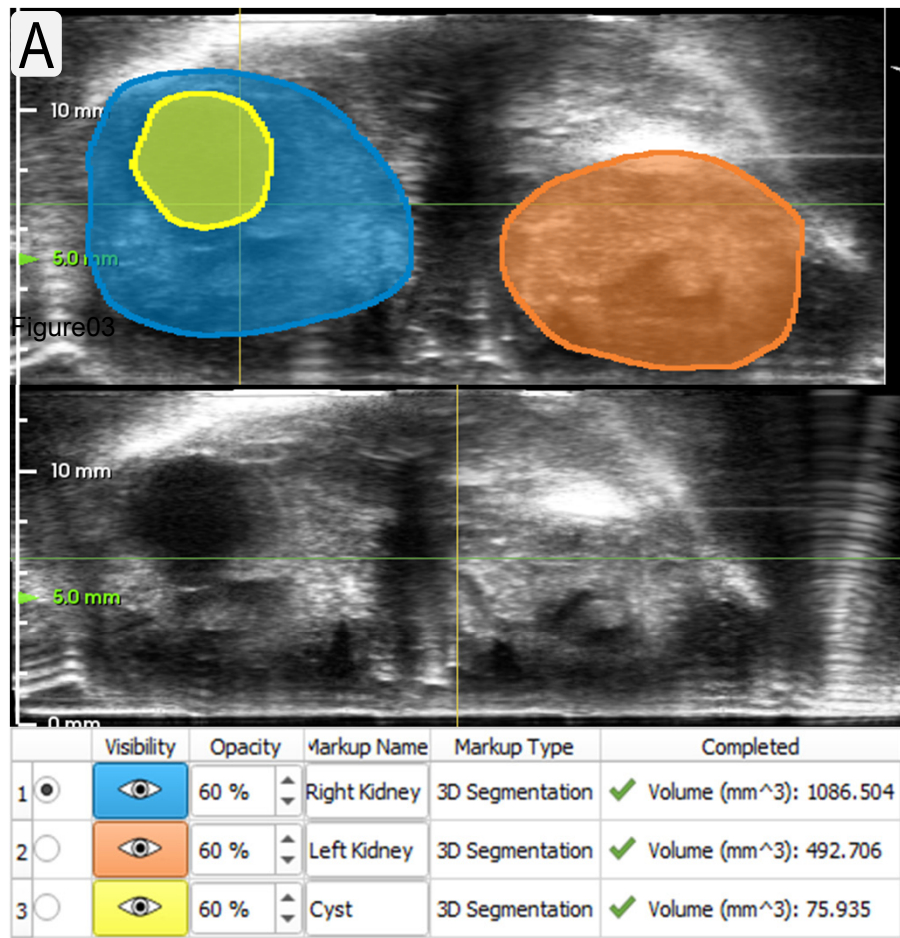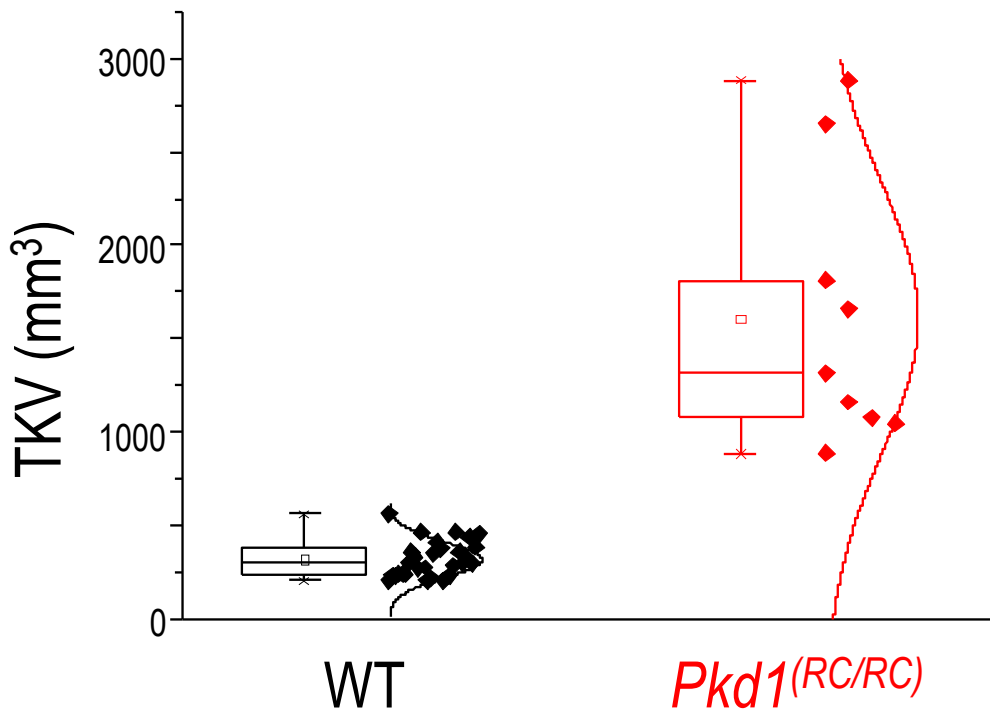| Ejection Fraction (%)	Stroke Volume (uL)	Heart Rate (BPM)
92.32721333	29.36433895	440.2362066
Cardiac Output (mL/min)	LV Volume;d (uL)	LV Volume;s (uL)
12.92724519	31.80464123	2.440302273
LV Mass (mg)	LV Internal Diameter;d (mm	LV Internal Diameter;s (mm)
273.4090416	2.885	1.065
LV Posterior Wall;d (mm)	LV Posterior Wall;s (mm)	LV Anterior Wall;d (mm)
2.473653755	3.11783442	1.236826877
LV Anterior Wall;s (mm)	Fractional Shortening (%)	LV Mass (corrected) (mg)
1.745729603	63.08492201	199.1146931

Figure 2

	Visibility	Opacity	Markup Name	Markup Type	Completed
1 ⊙	👁	60 %	Right Kidney	3D Segmentation	✓ Volume (mm^3): 1086.504
2 ○	👁	60 %	Left Kidney	3D Segmentation	✓ Volume (mm^3): 492.706
3 ○	👁	60 %	Cyst	3D Segmentation	✓ Volume (mm^3): 75.935

Axis 1 (a)	2.8165
Axis 2 (b)	2.677
Axis 3 (c)	2.3915
Volume (mm³)	75.53

Figure 3

		avg	sem	n	US-Kidney		
Genotype	PKD1	age (months)			TKV (US-sv) mm^3		
WT	+/+	18.0	0.8	22	279.1	14.7	19
PKD1-RC/RC	RC/RC	17.3	0.8	9	1610	240.8	9

Figure 4

Figure 5

Figure06

Genotype	PKD1	avg	sem	n	Cardiac											
		age (months)			Eject Frac(%)			Stroke Vol (uL)			HR(BPM)			CO (mL/min)		
WT	+/+	18.0	0.8	22	78.0	2.3	22	31.2	2.7	22	424	12	22	13.0	1.1	22
PKD1-RC/RC	RC/RC	17.3	0.8	9	80.6	3.5	9	27.8	5.5	9	422	26	9	11.4	2.3	9

Figure 6

A — Wild-type

B — Pkd1(RC/RC) — Cysts

C — Calcification model — Calcifications
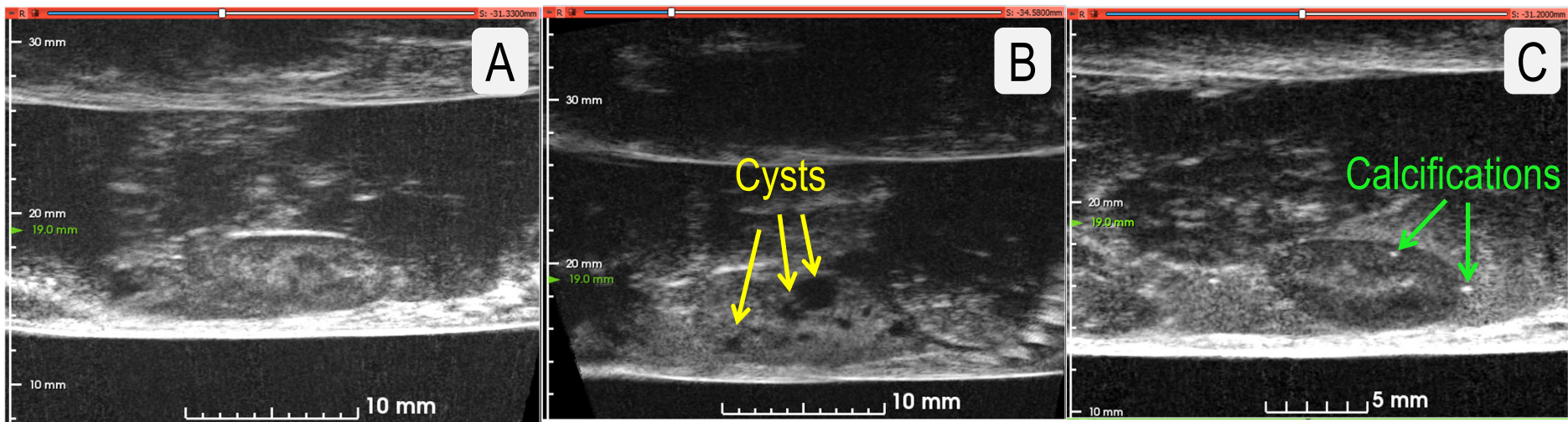
Figure07

Figure 7

Click here to access/download
Table of Materials
Table of Materials- 62682_R2.xlsx

Editorial comments:

Editorial Changes: *Changes to be made by the Author(s)*:

1. Please take this opportunity to thoroughly proofread the manuscript to ensure that there are no spelling or grammar issues.
Response: Article has been proofread thoroughly.

2. Please add more details to your protocol steps. Please ensure you answer the "how" question, i.e., how is the step performed? How is sufficient depth of anesthesia determined?
Response: Additional details have been added where appropriate.

3. The Protocol should be made up almost entirely of discrete steps without large paragraphs of text between sections. Please simplify the Protocol so that individual steps contain only 2-3 actions per step and a maximum of 4 sentences per step.
Response: Edited protocol so only 2-3 actions per step/maximum of 4 sentences are present in each step.

4. Please discuss all figures in the Representative Results in sequential order.
Response: Changed figure numbers so results will be discussed in sequential order.

5. Figure 5: Please include a space between the numbers and the units: TKV (mm3) instead of TKV(mm3).
Response: Added space between TKV and units.

6. Please spell out journal titles in all the references.
Response: Spelled out all journal titles in reference section.

Reviewers' comments:

Reviewer #1:

Manuscript Summary:

This paper reports on a method for the use of 3D robotic ultrasound for in vivo analysis of mouse kidneys and heart. The method is clearly described. This method would be useful for many investigators in the field.

Major Concerns:

None

Minor Concerns:

on line 140, "the" appears twice
Response: Deleted second "the" from that line.

Reviewer #2:

Manuscript Summary:

This manuscript utilizes the robotic controlled transducer in commercial SonoVol system to image multiple mice at once.

Major Concerns:

The words "robotic" and "transducers" have been mentioned multiple times in the text. But it is unclear in Fig. 1 where the transducer is and how the transducer is robotic controlled.

- Were 3D images acquired by moving the transducer along the mouse's body? How many degrees of freedom does the robotic transducer have? Can the transducer move around the belly without moving the mouse or deforming its shape?

Response:

- Added an additional panel in **Figure 1** to clearly show the location of the transducer.
- Also added information explaining the degrees of freedom of the transducers and how they move independently of the animal.

Editorial comments:
1. The manuscript file has been formatted to fit the journal standard. The personal pronouns are replaced in the manuscript text. Please check and verify.
Response: Changes look correct.

2. Please remove the commercial terms from the manuscript text (Vega, SonoVol, etc.). The commercial terms can be included in the Table of Materials.
Response: Removed commercial terms from manuscript text.

3. Comments to be addressed are included in the manuscript file. Please make the necessary changes.
Response: Addressed highlighted comments in manuscript file.

4. Please highlight up to 3 pages of the Protocol (including headings and spacing) that identifies the essential steps of the protocol for the video, i.e., the steps that should be visualized to tell the most cohesive story of the Protocol. Remember that non-highlighted Protocol steps will remain in the manuscript, and therefore will still be available to the reader.
Response: Highlighted most important steps of protocol.

5. Please include some limitations of the US system in the Discussion section.
Response: (now included in 2nd last paragraph in MS)
Some additional limitations of the system include:
- Only one linear array (centered at 18 MHz) is included in the robotic chassis, so switching to higher or lower frequency probes is not currently possible. This may impact the breath of models (either larger or smaller) that can be evaluated with the system. Future iterations of the instrument should include multiple linear arrays to cover the full range of preclinical animal models.
- The transducer angle relative to the animal subject cannot be controlled. Therefore performing angle-dependent imaging techniques, such as Doppler, or achieving alternative in-plane views of certain organs (e.g. long axis view of kidney) requires repositioning of the animal and can be difficult to achieve. Additional degrees-of-freedom could be added to the robotic movement to ameliorate this challenge.
- On occasion, we have observed reverberation artifacts arising from the acoustic membrane that separates the animal from the transducer that can obscure visualization of superficial features and boundaries. Using a gel standoff to elevate the animal away from the membrane can remedy these situations.
- Temperature control via heat lamp is imprecise, and therefore close attention must be paid to the animal's core body temperature while imaging. More controlled heating mechanisms, such as an integrated heating pad, will likely improve homeostasis management and imaging throughput.

6. Figure 1: Please remove the commercial term from the figure (SonoVol).
Response: Removed logo from Figure.

7. Figure 4/5: The figure legends and the figure do not match. They look interchanged. Please check and make the necessary changes.
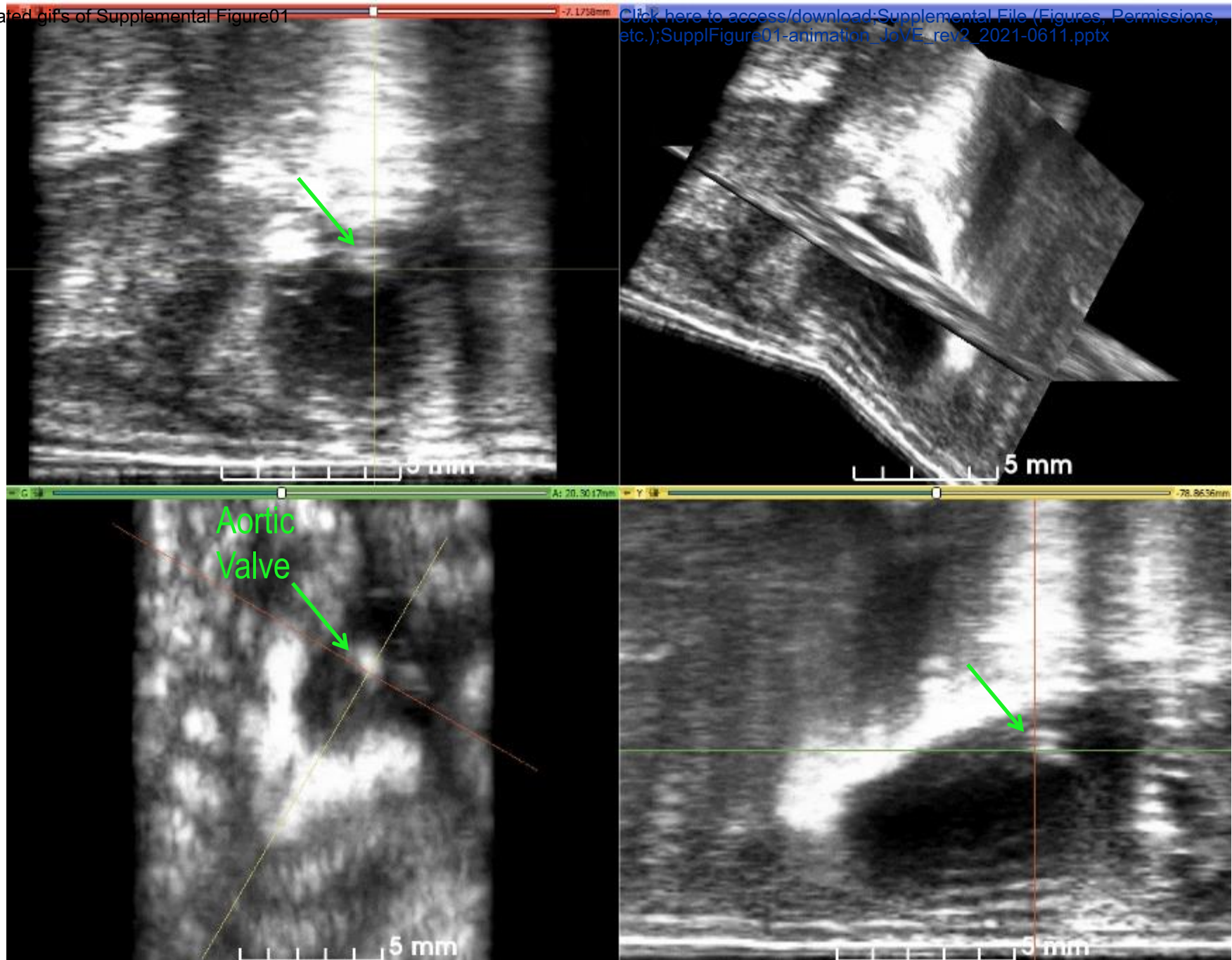Response: Checked figure legends and made sure they match.

8. For the 3D animated reconstruction, please define the colors differentiating the structures in the figure in the figure legends.
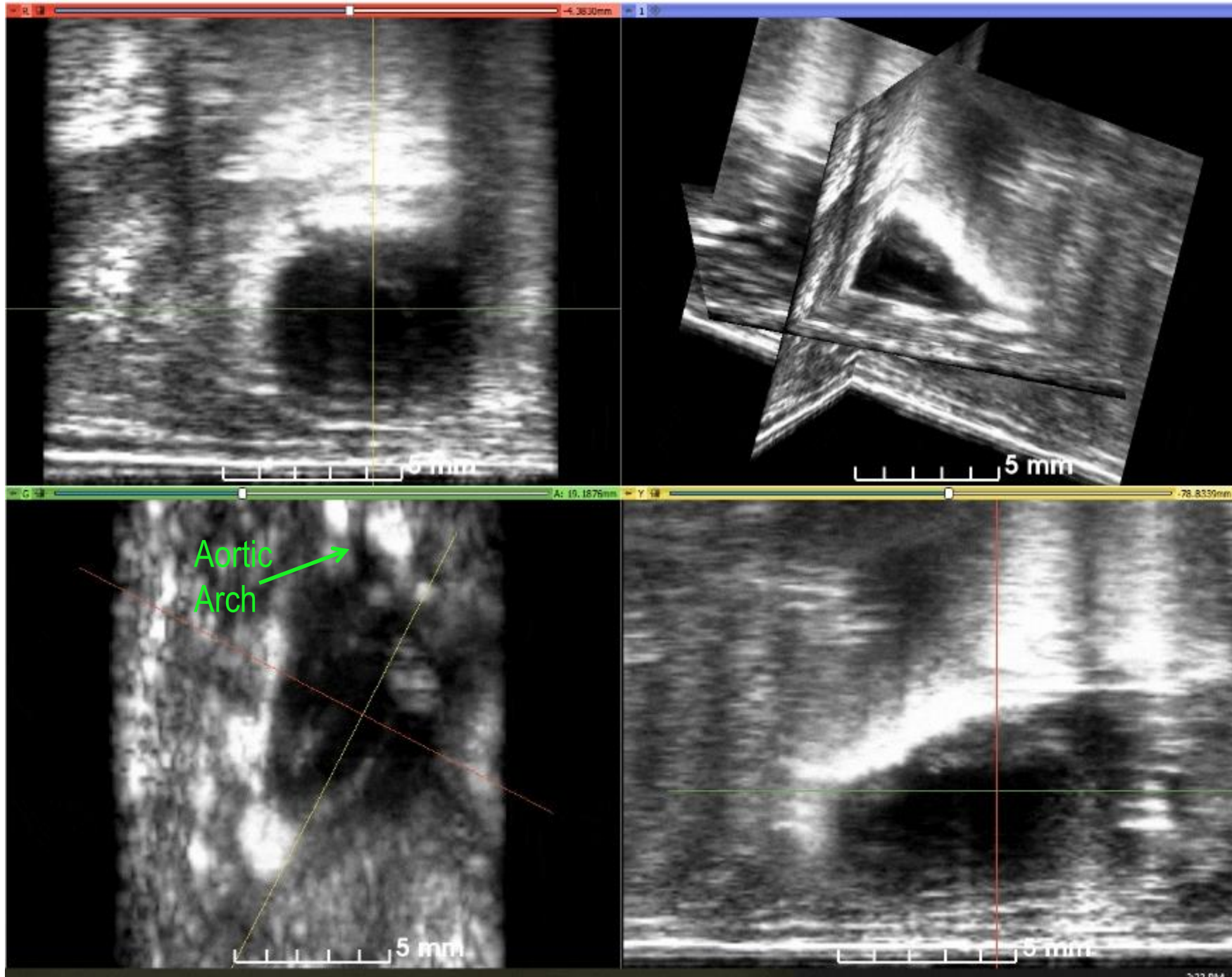Response: Added color definitions to figure legend.

9. Both screenshot and the 3D animated reconstruction of the kidneys are uploaded. Are both files necessary? If so, please add a title and a brief description for the animated 3D reconstruction in the figure legends. Please check and ensure whether it is Figure 4 or Figure 5 and rename the file accordingly.
Response: Should just be the animated 3D file (gif) for Figure 5. Figure 4 is the box plot of TKV distribution. Note Supplemental Figure 1 is also an animated Gif.

Supplemental Figure 1

Aortic
Arch

5 mm

5 mm

5 mm

5 mm

Supplemental Figure 2